LANGMUIR

pubs.acs.org/Langmuir Article

Urea Disrupts the AOT Reverse Micelle Structure at Low Temperatures

Samantha L. Miller* and Nancy E. Levinger*



Cite This: Langmuir 2022, 38, 7413–7421



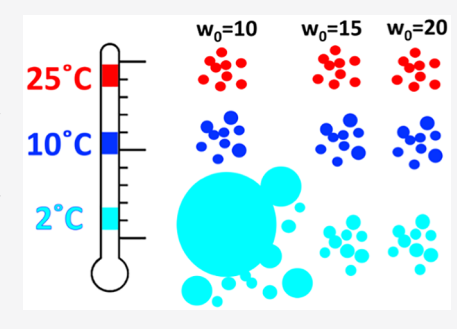
ACCESS

III Metrics & More

Article Recommendations

SI Supporting Information

ABSTRACT: Aside from its prominent role in the excretory system, urea is also a known protein denaturant. Here, we characterize urea as it behaves in confined spaces of AOT (sodium bis(2-ethylhexyl) sulfosuccinate) reverse micelles as a model of tight, confined spaces found at the subcellular level. Dynamic light scattering revealed that low temperatures (275 K) caused the smallest of the reverse micelle sizes, $w_0 = 10$, to destabilize and dramatically increase in apparent hydrodynamic diameter. We attribute this to urea embedded into the surfactant interface as confirmed by 2D ¹H-NOESY NMR spectroscopy. This increase in size in turn caused the hydrogen exchange between urea and water within the nanosized reverse micelles to increase as measured by 1D EXSY-NMR. A minimal enlarging effect and no increase in hydrogen exchange were observed when aqueous urea was introduced into $w_0 = 15$ or 20 reverse micelles, suggesting that this effect is unique to particularly small-diameter spaces (\sim 7 nm).



INTRODUCTION

Urea in aqueous solutions presents unique properties that are relevant to many different scientific communities. Aside from being highly water-soluble, ¹ urea has been shown to enhance the solubility of hydrocarbons in water, ²⁻⁴ cause proteins to denature, ^{5,6} and prevent micellar aggregation ^{7,8} by mediating the critical micelle concentration of various surfactants. ^{9,10} Because of these findings, numerous studies abound that examine how urea perturbs the local hydrogen bond network of water. ^{11,12}

Both simulations and experiments have spearheaded the effort to describe urea-in-water solutions. Within the biochemical community, urea is well known to denature proteins, 6,13 and as an osmolyte, urea has a unique effect on the traditional hydrogen bonds in bulk urea-in-water solutions. ^{12,14,15} For example, molecular dynamics simulations have generally shown that an increasing urea mole fraction disrupts the elaborate threedimensional tetrahedral framework of the water hydrogen bond network, leading to differences in solvation abilities. 12,14 Cabellero-Herrera et al. used molecular dynamics simulations to show that the denaturing effect of urea on proteins could be attributed to the decreased mobility of water in the presence of urea. 15 This simulation also reported an increase in water peptide bonds as a result of urea's presence, which destabilized the hydrogen bonds that would otherwise stabilize the α -helix structures within the protein. Coupled with experimental neutron diffraction studies, molecular dynamics simulations show that urea readily inserts itself into water and can form hydrogen bonds at both carbonyl and amine functional groups, as shown in Scheme 1. 16 Further neutron diffraction investigations by Kameda et al. found that such small intermolecular distances between oxygen atoms within the

Scheme 1. Labeled Chemical Structures of the AOT Surfactant Molecule and the Planar Urea Molecule Used in This $Study^a$

^aTwo-dimensional ¹H-NOESY NMR experiments indicate that the hydrogens explicitly shown in red interact with urea. These assignments have been made with previous literature studies. ⁴⁰.

water hydrogen bond network confirmed the breakdown of the tetrahedral water network. 17

Despite these studies that label urea as a structure breaker, others have suggested that urea is actually a structure maker based on a Kirkwood-Buff analysis; that is, urea stabilizes the self-association of water. ¹⁸ Investigations of urea and water solutions have also included spectroscopy studies, where both transient absorption and time-resolved IR experiments show a

Received: January 25, 2022 Revised: May 9, 2022 Published: June 7, 2022





sensitive response to the local solvent structure and its changes over time. $^{19-22}$

Considering the rich network of studies describing urea-inwater solutions, we focus on changes brought to this system by nanoconfinement that mimicks the intracellular spaces where urea is biologically active. It is well documented that nanoconfined water displays markedly different characteristics when compared to its bulk behavior. 23,24 Water confinement within nanosized spaces has been achieved through various means, including carbon and lipid nanotubes, 25-28 silica-based pores, ²⁹⁻³¹ and aerosolized particles. ^{32,33} In this study, we achieve nanoconfinement using reverse micelles, which are sizetunable nanodroplets that form spontaneously after the perturbation of a three-part mixture that includes a nonpolar solvent, polar solvent, and surfactant molecule. Reverse micelles are a popular choice for mimicking biological spaces with limited amounts of water such as intercellular and intraorganelle spaces, the interiors of macromolecular transport vesicles, or transport proteins and aquaporins.^{34,35} They also complement the emerging interest in nanofluidic devices.³⁶ The reverse micelle size is described by a unitless parameter $w_0 = [H_2O]/$ [surfactant] that describes the water loading ratio relative to the amount of surfactant. In the work reported here, we prepared reverse micelles with AOT surfactant with $w_0 = 10$, 15, and 20, which generally creates reverse micelles that are \sim 5-12 nm in diameter. AOT, whose structure is shown in Scheme 1, is an attractive surfactant because of the ease of reverse micelle preparation, thermodynamic stability, and the fact that it is inexpensive and nontoxic.

Previous experiments have studied urea in micelles and reverse micelles with varying results. For example, spectro-fluorometer scattering data show that low concentrations (<1.0 M) of urea appear to stabilize the AOT reverse micelle structure, and the chemical structures of both molecules are shown in Scheme 1.8,37 Ceraulo et al. has reported that urea interacts with the sulfonate headgroup through a hydrogen bond with urea's amino group and also showed that urea caused a differentiation between the two hydrocarbon chains comprising the AOT surfactant which then had distinct solubilizing roles. Second to demonstrate that urea in AOT reverse micelles began to interact with the hydrophilic headgroups of the AOT molecule and created greater disorder within the inner hydrogen bond network.

To date, studies of urea in reverse micelles have not taken into consideration the effect of variable temperature on either the interaction of urea with the reverse micelle surfactant or the inner water pool. By coupling techniques such as dynamic light scattering (DLS) and one- and two-dimensional NMR spectroscopy, we extend the current description of how nanoconfinement affects both the structure and dynamics of these rich systems. NMR techniques are extremely sensitive to changes in the chemical environment, making this union of technique and research question ideal. Urea is an attractive molecule for insertion into the reverse micelle water interior because the key analyte peaks do not overlap with the known resonances of either the surfactant or nonpolar solvent isooctane. Furthermore, knowledge of the chemical shift, resonance line widths, relaxation rates, and exchange rates can illuminate the mechanisms of transport occurring where nitrogenous waste is expelled via concentration gradients created within the vasculature of the kidneys.⁴¹

MATERIALS AND METHODS

Urea (99.9%), aerosol OT (AOT, (bis(2-ethylhexyl) sulfosuccinate sodium salt, 99.9%), 2,2,4-trimethylpentane (isooctane, 99.9%), and cyclohexane- d_{12} (99.9%) were purchased from MilliporeSigma (Burlington, MA) and used as received. $\rm D_2O$ (99.9%) was acquired from Cambridge Isotope Laboratories. We refer to 2,2,4-trimethylpentane as isooctane throughout this article. All water used in the experiment was Millipore filtered for 18 $\rm M\Omega$ cm resistivity. Prior to use, all glassware, including NMR tubes, was acid washed with concentrated HNO3, copiously rinsed with Millipore-filtered water, and thoroughly dried

Samples of reverse micelles were prepared from 0.1 M AOT stock solutions in isooctane with subsequent additions of water and then osmolyte. Solid AOT was added by mass to the isooctane solvent to achieve a 0.1 M concentration. Next, water was added to form the reverse micelle nanodroplets with the desired w_0 value and sonicated. Urea was loaded by mass to achieve a 1:30 urea/water mole ratio and further sonicated for ~50 min until complete emulsification was achieved. Although the concentration of the osmolytes within the reverse micelles was ~2 M, the overall urea concentration was 30 mM. Urea concentrations specific to each w_0 value are provided in Table S1.

Size measurements were used to evaluate the reverse micelle stability and the environment that the encapsulated osmolyte experiences. Reverse micelle formation and sizes were evaluated as a function of temperature using dynamic light scattering (Malvern Zetasizer Nano ZS) in backscattering mode (173°). Measurements were performed in triplicate to extract the average size across 30 scans. The lower temperature limit of the instrument precluded measurements below 275 K, which prevented measurements that mirrored the lowest temperatures probed in NMR studies. The reported error in the internal thermometer was ± 0.2 K. A five min equilibration time between measurements ensured homogeneous temperatures throughout the aqueous sample.

Viscosity data crucial to extracting accurate size measurements of reverse micelle samples were collected as a function of temperature using a Cannon-Fenske 9721-B74 (Cole Parmer) viscometer. A temperature-controlled water bath accurate to 0.1 K and an electronic timer assisted the measured efflux through the Ubbelohde glass tube. Each of the five viscosity measurements of 0.1 M AOT was repeated in triplicate (Figure S1 and Table S2)

Both ^1H and 1D EXSY-NMR spectra were collected using a Varian Inova 500 MHz spectrometer (Agilent) operating at 11.75 T. Two-dimensional ^1H -NOESY spectra were collected on a Bruker Neo 400 MHz spectrometer operating at 9.40 T using a prodigy cryoprobe with a 200 ms mixing time. Sample tubes containing reverse micelle mixtures were mixed with a cyclohexane- d_{12} lock solvent (2% by volume). Preparations for bulk solutions of urea used D_2O as the lock solvent. T1 relaxation measurements were conducted at both 298 and 275 K and resulted in calculated values of 3.1 and 2.4 s, respectively. To thoroughly evaluate the effect of temperature, spectra were collected between -21 and 30 $^\circ$ C. A methanol thermometer was used to calibrate and confirm the operating temperature before and after EXSY data collection. The samples and NMR probe were allowed to equilibrate for 30 min before experiments were performed to ensure the thermal stability of the NMR probe and the sample throughout the measurement.

All NMR spectra were processed in MNOVA (ver. 12.0.4-22023). The size of the direct NMR FIDs was 32 768 data points. All spectra were zero filled to twice the number of data points and apodized with a 1.00 Hz exponential weighting function. Individual peaks were fitted with Lorentzian—Gaussian line shapes using MNOVA software and subsequently integrated. Integrated intensities were used to follow the chemical exchange between water and urea and were analyzed using custom-written code in Matlab (MatLab ver. R2021b). Additional details about the EXSY-NMR experimental parameters can be found in the SI.

RESULTS AND DISCUSSION

Particle Size by Dynamic Light Scattering. We used dynamic light scattering (DLS) data to evaluate the reverse

micelle size as a function of temperature. Viscosity data used in these measurements are provided in Figure S2. We examine w_0 = 10, 15, and 20 reverse micelles at temperatures of between 275 and 303 K (Figure 1). As expected, a typical urea micelle's

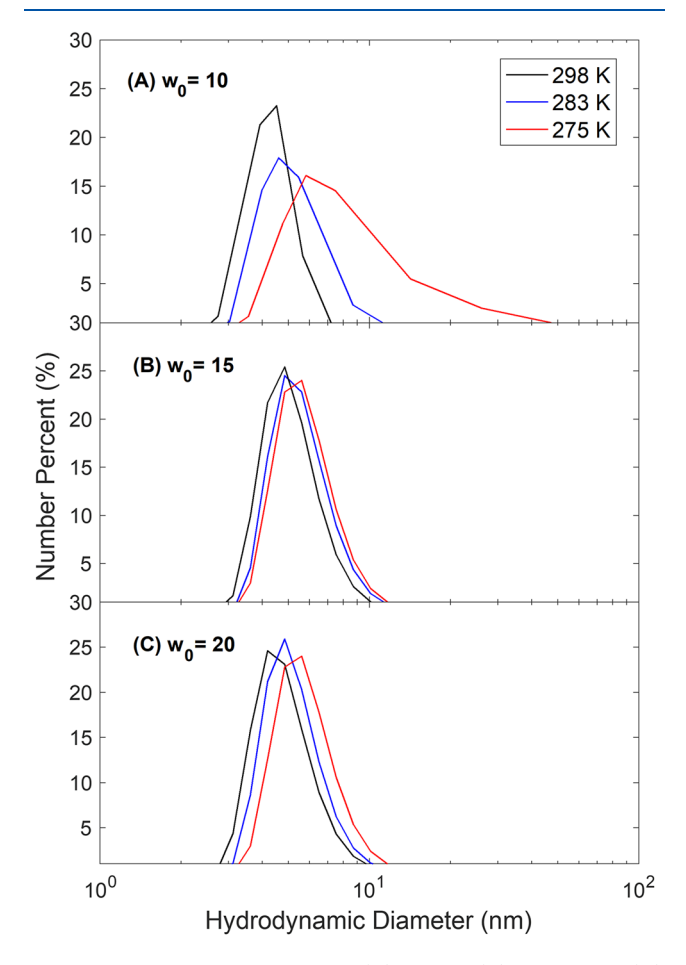


Figure 1. Dynamic light scattering of (A) $w_0 = 10$, (B) $w_0 = 15$, and (C) $w_0 = 20$ AOT reverse micelles with 1:30 urea/water as a function of temperature: T = 299 K (black), 283 K (blue), and 275 K (red).

apparent hydrodynamic diameter measured 5-12 nm. As temperature is initially ramped down to the lower limit of the instrument, we note that reverse micelles of all w_0 values grow larger and more disperse with no hysteresis. That is, the size and polydispersity for individual reverse micelle samples are conserved regardless of whether the temperature was achieved via cooling or warming. For the smallest reverse micelles measured, $w_0 = 10$, DLS scans reveal a dramatic effect of low temperature on the samples; at the instrument's low-temperature limit of 275 K, the reverse micelle size and polydispersity increase to the point where the solution contains reverse micelles that are as large as 50 to 100 nm, increasing from the size at room temperature by nearly an order of magnitude. In one particular experiment, a shoulder centered at about 20 nm appeared during the temperature-ramping period, suggesting that low temperature favors the formation of larger micelles.

Molecular Interaction by Two-Dimensional ¹H-NOESY NMR **Spectroscopy.** Two-dimensional ¹H-NOESY NMR spectra were collected at 275 and 298 K for reverse micelles at all w_0 values examined, i.e., 10, 15, and 20, to assess the intermolecular interactions between urea and AOT. Reference 1D ¹H-NMR spectra of $w_0 = 10$ reverse micelles at varying temperatures are provided in Figure 2. Although the spectral quality declines with decreasing temperature, features associated with urea, water, and AOT protons remain easily detected.

Two-dimensional ¹H-NOESY spectra of the $w_0 = 10$ reverse micelles shown in Figure 3 predictably show cross peaks between urea NH protons at ~6 ppm and water at ~4.5 ppm at both temperatures measured. In Figure 3B, additional cross peaks appear between the AOT headgroup CH peaks and the urea NH peak, demonstrating that urea interacts with the AOT headgroup CH protons at 275 K. These headgroup protons are shown explicitly via red highlighting in Scheme 1. In contrast, only water—urea cross peaks appear in the 2D ¹H-NOESY spectra for $w_0 = 15$ and 20 reverse micelles at both 275 and 298 K with no cross peaks between urea and the AOT headgroup CH protons at any temperatures probed (Figures S2 and S3).

Kinetic Model. In previous experiments, we have measured the exchange between water and hydroxyl groups on sugars and sugar alcohols, noting a significant slowing down of the exchange when these molecules are encapsulated in reverse micelles. 40,42,43 We also found evidence for two different regimes

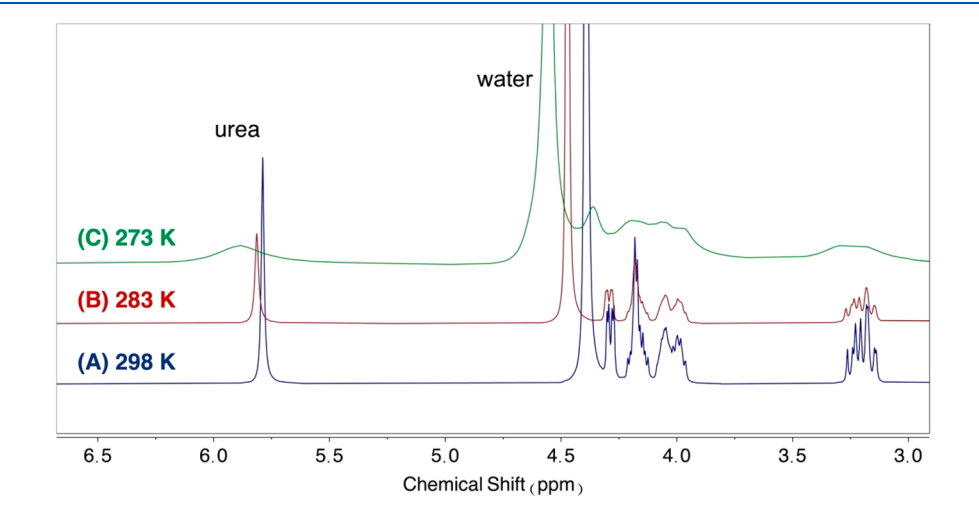


Figure 2. One-dimensional 1 H-NMR spectra of $w_0 = 10$ reverse micelles at varying temperatures containing the labeled peaks of interest used to analyze both the 2D 1 H-NOESY NMR spectra and the EXSY NMR spectra. Spectra at different temperatures are offset for ease of viewing.

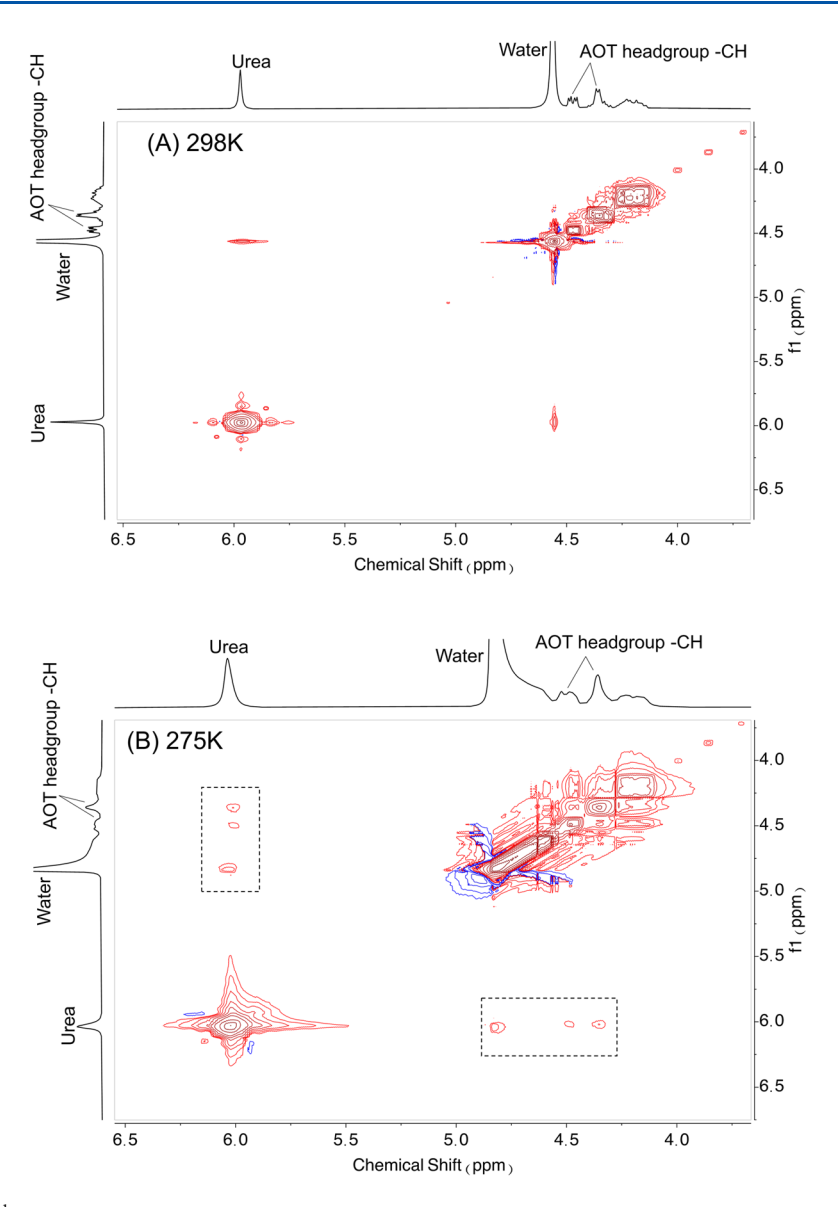


Figure 3. Two-dimensional ¹H-NOESY NMR spectra showing the region of interest for $w_0 = 10$ AOT reverse micelles encapsulating 2 M aqueous urea at (A) 298 K and (B) 275 K. At 298 K, cross peaks between water and urea predictably appear off the diagonal. At 275 K, additional cross peaks suggesting a urea-AOT headgroup interaction appear and are boxed in dotted lines for clarity.

wherein the exchange between water and glucose follows expected Arrhenius behavior at higher temperatures but appears to tunnel at a modestly low temperature of around 273 K. Here we explore the chemical exchange between water and urea in bulk aqueous solution and in AOT reverse micelles. The water—urea chemical exchange rate has been reported for bulk aqueous solutions. The planar urea molecule possesses four labile hydrogens that are bonded to the nitrogen of the primary amide groups flanking the central carbonyl, as shown in Scheme 1. The urea protons are subject to exchange with water and appear consistently at ~6 ppm in the NMR spectra. The exchange process between water and urea is described in eq 1:

$$HOH^* + NH \stackrel{k_1}{\rightleftharpoons} HOH + NH^* \stackrel{k_2}{\rightarrow} HOH + NH$$
 (1)

Here, HOH represents water, NH represents the labile urea hydrogen, and HOH* represents the hydrogen on water that has been labeled with a radio frequency pulse during the 1D EXSYNMR pulse sequence. (See the SI EXSY-NMR experimental

description.) Initially, the system contains only the labeled hydrogens on water and the unlabeled urea hydrogens. Once the labeled hydrogens have exchanged, the H* no longer appears on HOH but on NH*, signifying its exchange with the urea amide group. Eventually, the system returns to equilibrium as spinlattice relaxation dissipates the energy out of the system. Integration of the EXSY-NMR NH peak provides a relative measure of the NH* concentration. Using a range of mixing times in the EXSY-NMR pulse sequence allows us to measure the time dependence of the exchange process. Initially, the reverse micelle system consists of water and urea. During the pulse sequence, the water hydrogens are energetically labeled with a soft radio frequency pulse, as denoted by the asterisk (HOH*). We use rate constant k_1 to quantify the rate of hydrogen exchange from water to urea and k_{-1} to indicate the reverse process. Eventually, the radio frequency energy used to label hydrogens dissipates out of the system at a rate described by k_2 . Assuming that $k_1 \gg k_{-1}$, we obtain the rate equation, eq 2,

$$[NH^*] = \frac{k_1}{k_2 - k_1} [NH]_o (e^{-k_1 t} - e^{-k_2 t}) e^{-t/T_1} + C$$
(2)

which describes the intensity of the urea NH peaks during the exchange process. The exponential decay factor including T_1 accounts for water spin—lattice relaxation that can occur before the chemical exchange process begins and C is a constant offset associated with the solution to the differential equation.

Chemical Exchange Measurement by EXSY-NMR. Figure 4 shows representative data of the integrated intensity

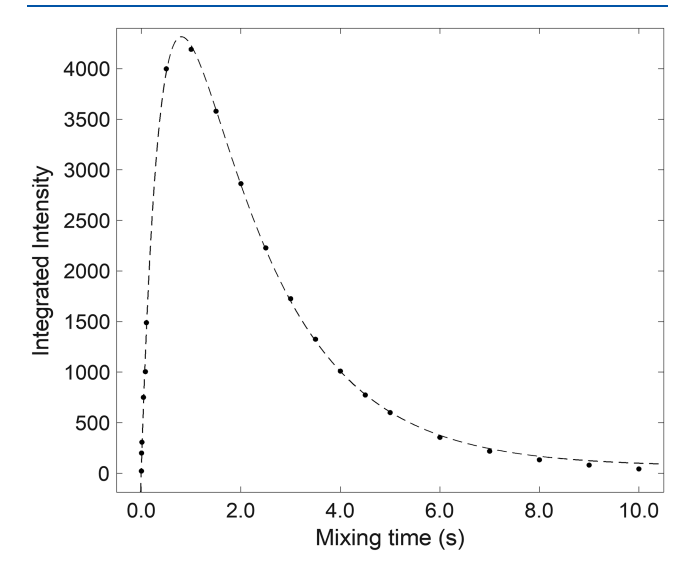


Figure 4. Integrated intensity of the EXSY-NMR peaks as a function of mixing time (points) and the fit to eq 2 (dashed line) at 298 K (25 $^{\circ}$ C) for $w_0 = 10$ reverse micelles containing 2 M urea (1:30 urea/water).

of the urea NH* signal as a function of mixing time determined from the EXSY-NMR spectra of $w_0 = 10$ AOT reverse micelles with a 1:30 urea/water mole ratio collected at 298 K. (Raw EXSY-NMR traces are shown in Figure S4.) The initial rise in the data points in Figure 4 indicates the rapid exchange of the labile hydrogen atom; it is followed by relaxation to chemical equilibrium that occurs for both bulk and nanoconfined urea solutions. We fit these data to eq 2 to obtain values for rate constants; values for k_1 exchange constants for all temperatures and w_0 values are given in Table 1. The exchange rates between water and urea in bulk aqueous solution and in $w_0 = 20$ reverse micelles are the same within our error, with slightly lower rates

Table 1. First-Order Exchange Rate Constants, k_1 , Measured by EXSY-NMR Spectroscopy at Various Temperatures^a

T(K)	$w_0 = 10 \text{ RMs}$	$w_0 = 15 \text{ RMs}$	$w_0 = 20 \text{ RMs}$	bulk 2 M urea
303	2.1 (±0.4)			
298	$2.3 (\pm 0.3)$	$4.7 (\pm 2.0)$	$11.9 \ (\pm 2.0)$	15.3 (±3.1)
293	$2.3 (\pm 0.3)$			
288	$2.5 (\pm 0.6)$			
283	$3.0 (\pm 0.5)$			
273	$3.2 (\pm 0.7)$	$3.9 (\pm 0.6)$	$7.8 \ (\pm 0.8)$	$8.6 (\pm 1.1)$
268	$3.5 (\pm 0.8)$			
263	4.3 (±0.7)	$2.0\ (\pm0.4)$		
252	$6.0 (\pm 1.1)$		$4.6 \ (\pm 0.9)$	$3.5 (\pm 0.8)$

"Rate constants determined from data fits to eq 2 are given in s⁻¹ and represent the average of three measurements of the same sample. The standard deviations between measurements are given in parentheses.

for $w_0 = 15$. At high temperatures, the chemical exchange between water and urea is significantly slower for $w_0 = 10$ reverse micelles, but surprisingly, the rates increase with decreasing temperature. Additional extracted parameters such as the k_2 constant may be found in Table S3.

After conducting EXSY-NMR experiments at 298 K, we sought to measure the energy barrier to the water-to-urea chemical exchange. We conducted EXSY-NMR experiments over a range of temperatures for bulk aqueous urea (2 M) and for each w_0 value, w_0 value, 10, 15 and 20, to construct an Arrhenius plot. After collecting the k_1 exchange constant at these varying temperatures, we used the Arrhenius equation to extract E_A as shown in Figure 5. Each point on the Arrhenius plot represents

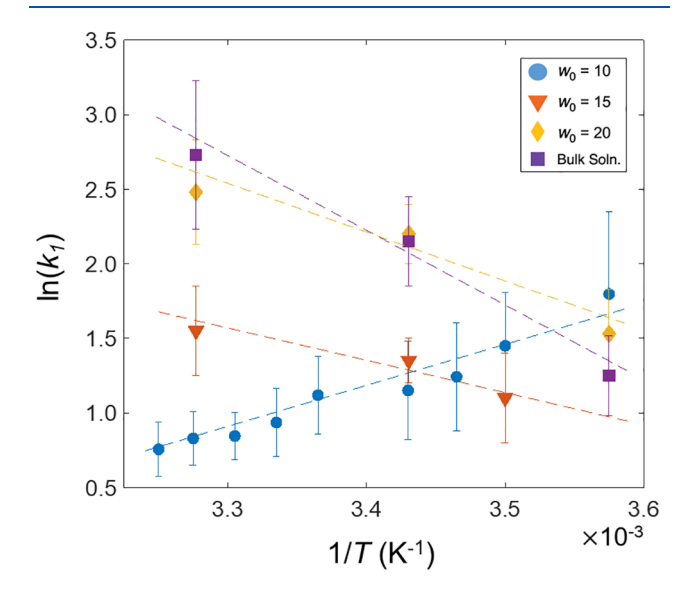


Figure 5. Arrhenius plots showing the hydrogen atom exchange rates between water and urea as a function of inverse temperature for AOT reverse micelles with $w_0 = 10$ (blue), 15 (orange), and 20 (gold) and bulk solution (purple). Dashed lines represent linear fits to the data. Error bars represent the standard deviation from three measurements of the same sample.

the average k_1 exchange constant collected from three experiments. Activation energy values are provided in Table 2. The measured activation energies of exchange between water and urea are highest for bulk aqueous urea solution and decrease as the reverse micelle size decreases.

■ DISCUSSION AND INTERPRETATION OF RESULTS

Our experiments on urea-containing reverse micelles indicate significant changes to the system as a function of water loading and temperature. We immediately ruled out the possibility of a

Table 2. Activation Energy Values Obtained from Arrhenius Plots a,b

w_0 value	$E_{\rm A}$ (kJ/mol)
10	$-12.4 \ (\pm 1.9)^c$
15	$7.6 (\pm 1.9)$
20	12.9 (±3.6)
bulk solution	20.0 (±2.5)

^aln k_1 as a function of 1/T. ^bThe reported error was calculated from the error in the slope of the linear fit. ^cThe apparent negative E_A value is interpreted in the Discussion and Interpretation of Results section.

freezing event considering that the EXSY NMR peaks would almost certainly broaden in response to a phase change. Furthermore, previous differential scanning calorimetry experiments with glucose-loaded reverse micelles showed no evidence of freezing. Considering that urea would act as a freezing-point depressant, the explanation of the size change must be independent of a phase-dependent response. Reverse micelle sizes measured by DLS suggest that urea destabilizes the small reverse micelles at low temperatures, as demonstrated by the substantial increase in particle size and polydispersity for the w_0 = 10 reverse micelles. In comparison, reverse micelles with higher water loading, either $w_0 = 15$ or 20, show only minor increases in size and polydispersity as the temperature drops. Our EXSY-NMR measurements indicate that the water-urea hydrogen atom exchange rate increases despite a decrease in temperature for the $w_0 = 10$ reverse micelles. In contrast, reverse micelles at higher water loading display the expected Arrhenius behavior of a slowing exchange rate with temperature. Combined, these results show that significant differences exist for the reverse micelles as the ratio between AOT surfactant and the polar solvent content decreases.

The proximity of urea molecules to the AOT headgroups at 273 K in the $w_0 = 10$ reverse micelles, as indicated by the 2D 1 H-NOESY data, could cause an increase in the apparent surface area of the surfactant interface. The tight intercalation of the urea molecules with the AOT headgroups could cause the largely cone-shaped geometry of the AOT surfactant molecules to become more cylindrical as the nested urea molecules create more bulk at the headgroup. This additional girth in the headgroup region could lead to an increased overall reverse micelle volume. This change in geometry is modeled in Figure 6, which demonstrates how the overlap of cone-shaped surfactant

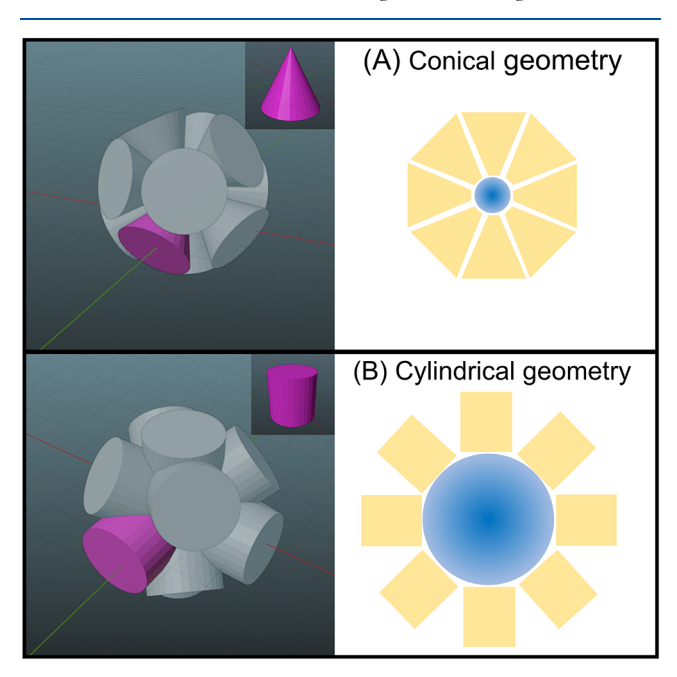


Figure 6. Two- and three-dimensional models representing the AOT surfactant molecule as (A) cones and (B) cylinders. The cone-shaped geometry permits tight packing of the surfactant around a small inner volume. However, as the 3D model at the bottom left shows, a switch to cylinders of the same height would create an overlap that is physically impossible and therefore results in an expanded inner water pool as shown in the 2D illustration.

cylinders forces the expansion of a larger overall water pool. Additionally, we note that the analysis of particles by DLS assumes a relatively spherical geometry, which is almost certainly a simplification of the true reverse micelle shape at any instant in time. ⁴⁵ It is likely that the larger average apparent hydrodynamic radius measured at lower temperatures indicates a change in morphology that does not perfectly scale with a spherical geometry and would also account for the vast increase in polydispersity.

The EXSY-NMR data collected can provide a measure of the relative number of urea molecules exchanging protons with water. If urea molecules insert between the AOT headgroups at low temperatures such that the NH moieties interact with AOT headgroup protons as indicated by the 2D ¹H-NOESY NMR (Figure 3), then those NH groups would not be available to exchange with water molecules and would decrease the pool of urea molecules available for exchange. This should depress the overall area of the urea peak relative to the water peak observed in the EXSY-NMR spectra. Because these embedded urea molecules no longer participate in exchange, they are not detected by the EXSY-NMR experiment. To provide quantitative evidence to support this hypothesis, we evaluate the ratio of the integrated urea peak to the water peak intensity in the EXSY-NMR spectra. A low urea/water peak intensity ratio indicates less urea available for exchange; a high urea/water ratio indicates more urea available for exchange. Table 3 presents a summary of this ratio analysis with the standard deviations provided calculated from the residual errors in line fitting.

Table 3. Ratio of the Urea Peak Integrated Intensity to the Water Peak Integrated Intensity from EXSY-NMR Measurements Determined for a Mixing Time of 1.0 s for AOT Reverse Micelles Containing 1:30 Urea/Water as a Function of w_0 and Temperature^a

	urea/water peak intensity ratio		
w_0 value	298 K	273 K	
10	0.10 (0.012)	0.009 (0.0014)	
15	0.11 (0.012)	0.032 (0.0046)	
20	0.10 (0.012)	0.029 (0.0042)	

"Ratios represent an average over the EXSY-NMR mixing times associated with the highest intensities where exchange occurs with the highest probability. Standard deviations are provided in parentheses.

With a fraction of the urea molecules removed from the exchange process, only the urea molecules remaining in the water pool will exchange with water. With a much larger water pool, the urea molecules could access a more bulklike environment, causing the exchange rate we measure to increase with decreasing temperature. The water pool for $w_0 = 10$ reverse micelles grows as a fraction of the urea molecules embeded in the interface, therefore providing a larger water pool for urea molecules remaining in the water environment. The urea molecules remaining in the water pool display a faster exchange rate. Table 3 shows that the ratio of the EXSY NMR peak intensity for urea/water is consistently larger at 298 K than it is at 273 K for all w_0 sizes at a mixing time of 1.0 s. This indicates that more hydrogen exchange between water and urea is occurring at higher temperatures. For $w_0 = 10$ reverse micelles, the ratio of urea peak intensity to water peak intensity at 273 K decreases by more than a factor of 10, supporting our hypothesis that significantly less urea is available for hydrogen exchange. The values indicated in Table 3 also demonstrate that although

 k_1 and k_2 vary across the different w_0 sizes, the urea/water peak ratios at maximum intensity are nearly identical. This confirms that any interference from the instantaneous rate of exchange does not arise from the kinetic behavior of the system as a whole.

Our interpretation of urea insertion into the AOT reverse micelle interface is also consistent with the observation of cross peaks in the 2D ¹H-NOESY NMR spectra that indicate urea has inserted itself into the interfacial region among the AOT surfactant headgroups. In contrast, for $w_0 = 15$ and 20 reverse micelles the ratio in the integral of urea/water EXSY-NMR peaks decreases by only a factor of \sim 3 as the temperature drops from 298 to 273 K. Lower temperatures also result in a lower S/ N ratio; this adds uncertainty to the smaller urea peak more than the consistently intense water peak. However, the residual values shown in Table S4 demonstrate that highly accurate integrations were still obtained. It is possible that the urea molecules begin to embed in the interface as temperature drops for all reverse micelle samples measured; this could account for the slight increase in size observed for $w_0 = 15$ and 20 reverse micelles at lower temperatures. In this case, we might expect to observe cross peaks between the AOT headgroups and urea in the 2D ¹H-NOESY spectra collected at low temperatures for $w_0 = 15$ and 20, but the spectra show no hint of this interaction in these systems. However, a low S/N would likely preclude the small signals from being observed in the low-temperature 2D NOESY spectra. Most critically, comparing the much more dramatic decrease of the urea/water peak ratio for the $w_0 = 10$ reverse micelles at low temperatures to the other $w_0 = 15$ and 20 reverse micelles further supports our proposition that the higher exchange rates we measure at low temperatures for the w_0 = 10 reverse micelles are caused by urea molecules residing in the water pool available for enhanced exchange while many embed in the interface where they do not exchange.

Another explanation for an increased exchange rate could be from a change in intramicellar pH. At high and low pH values, the concerted H-atom exchange mechanism prevalent near neutral pH changes to a charge-transfer mechanism, which can be orders of magnitude faster. 46 Previous studies have hypothesized that if the pH of the aqueous phase in AOT reverse micelles diverges from neutral, then the interfacial region can be significantly more acidic or basic than the water core. 47 If urea affects the intramicellar pH and it resides at the interface, we might expect faster exchange to occur. However, when the charge-transfer mechanism is active, it also affects the NMR spectrum, pulling urea and water peaks closer to each other and eventually merging these peaks.⁴⁸ Though we do not observe merging peaks, the apparent rate constants we measure agree well with water-urea proton exchange studies reported by Stabinska et al. using water exchange (WEX) NMR spectroscopy. They measured both acid- and base-catalyzed exchange rates for aqueous urea solutions but could not measure exchange for the concerted mechanism. Their findings suggest that cooling the temperature of $w_0 = 10$ reverse micelles and therefore destabilizing the nanostructure of the enclosed space may be akin to titrating the pH so that exchange becomes acidor base-catalyzed.44

A change from concerted to an acid-/base-catalyzed mechanism could also account for the decreasing values of $E_{\rm A}$ from bulk aqueous solution to the reverse micelles. However, this mechanism does not explain the increasing rates observed with decreasing temperature or the larger sizes measured for all reverse micelles as a function of temperature. Our results demonstrate urea's destabilizing effect observed in other studies

that involve more complex biological environments. For instance, urea's disruption of AOT reverse micelle aggregation shares similarities with the observation that the denaturation of a bovine serum albumin begins when urea localized at the protein surface leads to a repulsion between urea and charged residues. It appears that the urea in our AOT reverse micelle systems follows a similar pattern of localization at a surface that can initiate significant structural changes.

CONCLUSIONS

We find that the restriction to nanosized reverse micelles has a modest effect on the hydrogen exchange behavior between water and urea relative to the bulk behavior. However, our experiments demonstrate that small reverse micelle values, w_0 = 10, at low temperatures show significant differences in the interaction of urea with the surfactant interface, leading to dramatic changes in the reverse micelle size. Specifically, urea appears to embed itself into the interfacial area in $w_0 = 10$ reverse micelles at temperatures at and below water's freezing temperature. This dramatically enlarges the reverse micelle apparent hydrodynamic diameter and allows the remaining urea molecules in the reverse micelle water core to display bulklike exchange behavior because all of the urea molecules that are exchanging experience a large intramicellar water pool. This effect was not observed for larger $w_0 = 15$ or 20 sizes. These results may have important biomedical implications because they indicate that unique urea interactions could occur within the confined environment of cellular mitochondria. 50 A closer examination of single hydrogen transfer may help to elucidate the mechanisms fundamental to physiological homeostasis.

ASSOCIATED CONTENT

Supporting Information

The Supporting Information is available free of charge at https://pubs.acs.org/doi/10.1021/acs.langmuir.2c00206.

Plot of the viscosity of 0.1 M AOT in isooctane as a function of temperature; table of extrapolated viscosity values for the viscosity of 0.1 M AOT in isooctane at the temperatures in this study; a description of the 1D EXSYNMR experiments; 2D 1 H-NOESY NMR spectra of w_0 = 15 and 20 reverse micelles as a function of temperature; example EXSY-NMR spectra for samples of 2 M urea in w_0 = 10 reverse micelles collected at 298 K; and a table of raw integration values obtained to calculate the urea/water ratio (PDF)

AUTHOR INFORMATION

Corresponding Authors

Samantha L. Miller — Department of Chemistry, Colorado State University, Fort Collins, Colorado 80523, United States; Email: Sam.Miller@colostate.edu

Nancy E. Levinger — Department of Chemistry and Department of Electrical and Computer Engineering, Colorado State University, Fort Collins, Colorado 80523, United States; orcid.org/0000-0001-9624-4867; Email: Nancy.Levinger@ColoState.edu

Complete contact information is available at: https://pubs.acs.org/10.1021/acs.langmuir.2c00206

Notes

The authors declare no competing financial interest.

ACKNOWLEDGMENTS

We gratefully acknowledge financial support from NSF grant 1956323 and the Colorado State University Analytical Resource Core, Research Resource ID (RRID: SCR_021758). We thank Prof. Joseph DiVerdi for help with viscosity measurements as well as Dr. David Osborne for stimulating and helpful discussions. Additionally, we honor the Colorado State University land acknowledgment, https://landacknowledgment.colostate.edu/.

REFERENCES

- (1) Barel, D.; Black, C. A. Effect of Neutralization and Addition of Urea, Sucrose, and Various Glycols on Phosphorus Absorption and Leaf Damage from Foliar-Applied Phosphate. *Plant Soil* 1979, 52 (4), 515–525.
- (2) Frank, H. S.; Franks, F. Structural Approach to the Solvent Power of Water for Hydrocarbons; Urea as a Structure Breaker. *J. Chem. Phys.* **1968**, 48 (10), 4746–4757.
- (3) Graziano, G. Size and Temperature Dependence of Hydrocarbon Solubility in Concentrated Aqueous Solutions of Urea and Guanidine Hydrochloride. *Can. J. Chem.* **2002**, *80* (4), 388–400.
- (4) Inoue, Y.; Niiyama, D.; Murata, I.; Kanamoto, I. Usefulness of Urea as a Means of Improving the Solubility of Poorly Water-Soluble Ascorbyl Palmitate. *Int. J. Med. Chem.* **2017**, 2017, 4391078.
- (5) Rossky, P. J. Protein Denaturation by Urea: Slash and Bond. *Proc. Natl. Acad. Sci. U. S. A.* **2008**, *105* (44), 16825–16826.
- (6) Bennion, B. J.; Daggett, V. The Molecular Basis for the Chemical Denaturation of Proteins by Urea. *Proc. Natl. Acad. Sci. U. S. A.* **2003**, 100 (9), 5142–5147.
- (7) Schiøtt, B.; Iversen, B. B.; Madsen, G. K. H.; Larsen, F. K.; Bruice, T. C. On the Electronic Nature of Low-Barrier Hydrogen Bonds in Enzymatic Reactions. *Proc. Natl. Acad. Sci. U. S. A.* **1998**, 95 (22), 12799–12802.
- (8) Thapa, U.; Ismail, K. Urea Effect on Aggregation and Adsorption of Sodium Dioctylsulfosuccinate in Water. *J. Colloid Interface Sci.* **2013**, 406, 172–177.
- (9) Kumar, S.; Parveen, N.; Kabir-Ud-Din. Effect of Urea Addition on Micellization and the Related Phenomena. *J. Phys. Chem. B* **2004**, *108* (28), 9588–9592.
- (10) Zangi, R.; Zhou, R.; Berne, B. J. Urea's Action on Hydrophobic Interactions. J. Am. Chem. Soc. 2009, 131 (4), 1535–1541.
- (11) Kallies, B. Coupling of Solvent and Solute Dynamics Molecular Dynamics Simulations of Aqueous Urea Solutions with Different Intramolecular Potentials. *Phys. Chem. Chem. Phys.* **2002**, *4* (1), 86–95.
- (12) Idrissi, A.; Gerard, M.; Damay, P.; Kiselev, M.; Puhovsky, Y.; Cinar, E.; Lagant, P.; Vergoten, G. The Effect of Urea on the Structure of Water: A Molecular Dynamics Simulation. *J. Phys. Chem. B* **2010**, *114* (13), 4731–4738.
- (13) Choa, H. S.; Dashdorj, N.; Schotte, F.; Graber, T.; Henning, R.; Anfinrud, P. Protein Structural Dynamics in Solution Unveiled via 100-Ps Time-Resolved x-Ray Scattering. *Proc. Natl. Acad. Sci. U. S. A.* **2010**, 107, 7281.
- (14) Stumpe, M. C.; Grubmüller, H. Aqueous Urea Solutions: Structure, Energetics, and Urea Aggregation. *J. Phys. Chem. B* **2007**, *111* (22), 6220–6228.
- (15) Caballero-Herrera, A.; Nordstrand, K.; Berndt, K. D.; Nilsson, L. Effect of Urea on Peptide Conformation in Water: Molecular Dynamics and Experimental Characterization. *Biophys. J.* **2005**, 89 (2), 842–857.
- (16) Soper, A. K.; Castner, E. W.; Luzar, A. Impact of Urea on Water Structure: A Clue to Its Properties as a Denaturant? *Biophys. Chem.* **2003**, *105* (2–3), 649–666.
- (17) Kameda, Y.; Amo, Y. Partial Pair Correlation Functions of Highly Concentrated Aqueous Urea Solutions Determined by Neutron Diffraction with 14N/15N and H/D Isotopic Substitution Methods. *Bull. Chem. Soc. Jpn.* **2010**, 83 (2), 131–144.
- (18) Chitra, R.; Smith, P. E. Molecular Association in Solution: A Kirkwood-Buff Analysis of Sodium Chloride, Ammonium Sulfate,

- Guanidinium Chloride, Urea, and 2,2,2-Trifluoroethanol in Water. J. Phys. Chem. B 2002, 106 (6), 1491–1500.
- (19) Ohta, K.; Tayama, J.; Saito, S.; Tominaga, K. Vibrational Frequency Fluctuation of Ions In. *Acc. Chem. Res.* **2012**, *45* (11), 1982–1991
- (20) Hoccart, X.; Turrell, G. Raman Spectroscopic Investigation of the Dynamics of Urea-Water Complexes. *J. Chem. Phys.* **1993**, 99 (11), 8498–8503.
- (21) Sharp, K. A.; Madan, B.; Manas, E.; Vanderkooi, J. M. Water Structure Changes Induced by Hydrophobic and Polar Solutes Revealed by Simulations and Infrared Spectroscopy. *J. Chem. Phys.* **2001**, *114* (4), 1791–1796.
- (22) Grdadolnik, J.; Maréchal, Y. Urea and Urea-Water Solutions An Infrared Study. *J. Mol. Struct.* **2002**, *615* (1–3), 177–189.
- (23) Knight, A. W.; Kalugin, N. G.; Coker, E.; Ilgen, A. G. Water Properties under Nano-Scale Confinement. *Sci. Rep.* **2019**, *9* (1), 1–12.
- (24) Alba-Simionesco, C.; Coasne, B.; Dosseh, G.; Dudziak, G.; Gubbins, K. E.; Radhakrishnan, R.; Sliwinska-Bartkowiak, M. Effects of Confinement on Freezing and Melting. *J. Phys.: Condens. Matter* **2006**, 1–68, DOI: 10.1088/0953-8984/18/6/R01.
- (25) Takaiwa, D.; Hatano, I.; Koga, K.; Tanaka, H. Phase Diagram of Water in Carbon Nanotubes. *Proc. Natl. Acad. Sci. U. S. A.* **2008**, *105* (1), 39–43.
- (26) Thostenson, E. T.; Ren, Z.; Chou, T. W. Advances in the Science and Technology of Carbon Nanotubes and Their Composites: A Review. *Compos. Sci. Technol.* **2001**, *61* (13), 1899–1912.
- (27) Iijima, S. Helical Microtubules of Graphitic Carbon. *Nature* **1991**, 354, 56–58.
- (28) Wilson-Kubalek, E. M.; Brown, R. E.; Celia, H.; Milligan, R. A. Lipid Nanotubes as Substrates for Helical Crystallization of Macromolecules. *Proc. Natl. Acad. Sci. U. S. A.* **1998**, 95 (14), 8040–8045.
- (29) Ilgen, A. G.; Kabengi, N.; Leung, K.; Ilani-Kashkouli, P.; Knight, A. W.; Loera, L. Defining Silica-Water Interfacial Chemistry under Nanoconfinement Using Lanthanides. *Environ. Sci. Nano* **2021**, 8 (2), 432–443.
- (30) Kumarasinghe, R.; Ito, T.; Higgins, D. A. Nanoconfinement and Mass Transport in Silica Mesopores: The Role of Charge at the Single Molecule and Single Pore Levels. *Anal. Chem.* **2020**, 92 (1), 1416–1423
- (31) Chowdhury, S. R.; Schmuhl, R.; Keizer, K.; Ten Elshof, J. E.; Blank, D. H. A. Pore Size and Surface Chemistry Effects on the Transport of Hydrophobic and Hydrophilic Solvents through Mesoporous γ -Alumina and Silica MCM-48. *J. Membr. Sci.* **2003**, 225 (2), 177–186.
- (32) Lee, J. K.; Banerjee, S.; Nam, H. G.; Zare, R. N. Acceleration of Reaction in Charged Microdroplets. *Q. Rev. Biophys.* **2015**, *48* (4), 437–444.
- (33) Ding, Y.; Riediker, M. A System to Create Stable Nanoparticle Aerosols from Nanopowders. *J. Vis. Exp.* **2016**, 2016 (113), 54414.
- (34) Palmer, N. J.; Eskici, G.; Axelsen, P. H. Non-Equilibrium Mass Exchange in AOT Reverse Micelles. *J. Phys. Chem. B* **2020**, *124* (1), 144–148.
- (35) Eskici, G.; Axelsen, P. H. The Size of AOT Reverse Micelles. *J. Phys. Chem. B* **2016**, *120* (44), *11337*–11347.
- (36) Yamamoto, K.; Ota, N.; Tanaka, Y. Nanofluidic Devices and Applications for Biological Analyses. *Anal. Chem.* **2021**, 93 (1), 332–349.
- (37) Chakraborty, A.; Sarkar, M.; Basak, S. Stabilizing Effect of Low Concentrations of Urea on Reverse Micelles. *J. Colloid Interface Sci.* **2005**, 287 (1), 312–317.
- (38) Ceraulo, L.; Dormond, E.; Mele, A.; Turco Liveri, V. FT-IR and Nuclear Overhauser Enhancement Study of the State of Urea Confined in AOT-Reversed Micelles. *Colloids Surfaces A Physicochem. Eng. Asp.* **2003**, 218, 255–264.
- (39) Caponetti, E.; Chillura-Martino, D.; Ferrante, F.; Pedone, L.; Ruggirello, A.; Liveri, V. T. Structure of Urea Clusters Confined in AOT Reversed Micelles. *Langmuir* **2003**, *19* (12), 4913–4922.
- (40) Wiebenga-Sanford, B. P.; Washington, J. B.; Cosgrove, B.; Palomares, E. F.; Vasquez, D. A.; Rithner, C. D.; Levinger, N. E. Sweet

Confinement: Glucose and Carbohydrate Osmolytes in Reverse Micelles. J. Phys. Chem. B 2018, 122 (41), 9555–9566.

- (41) Higgins, C. Urea and the Clinical Value of Measuring Blood Urea Concentration. *Acutecaretesting Org.* **2016**, No. August, 1–6.
- (42) Wiebenga-Sanford, B. P.; Diverdi, J.; Rithner, C. D.; Levinger, N. E. Nanoconfinement's Dramatic Impact on Proton Exchange between Glucose and Water. *J. Phys. Chem. Lett.* **2016**, *7* (22), 4597–4601.
- (43) Miller, S. L.; Wiebenga-Sanford, B. P.; Rithner, C. D.; Levinger, N. E. Nanoconfinement Raises the Energy Barrier to Hydrogen Atom Exchange between Water and Glucose. *J. Phys. Chem. B* **2021**, *125* (13), 3364–3373.
- (44) Stabinska, J.; Neudecker, P.; Ljimani, A.; Wittsack, H. J.; Lanzman, R. S.; Müller-Lutz, A. Proton Exchange in Aqueous Urea Solutions Measured by Water-Exchange (WEX) NMR Spectroscopy and Chemical Exchange Saturation Transfer (CEST) Imaging in Vitro. *Magn. Reson. Med.* **2019**, *82*, 935–947.
- (45) Gale, C. D.; Derakhshani-Molayousefi, M.; Levinger, N. E. How to Characterize Amorphous Shapes: The Tale of a Reverse Micelle. *J. Phys. Chem. B* **2022**, *126*, 953–963.
- (46) Hills, B. P. Multinuclear NMR Studies of Water in Solutions of Simple Carbohydrates. *Mol. Phys.* **1991**, *72* (5), 1099–1121.
- (47) Afzal, S.; Lone, M. S.; Nazir, N.; Dar, A. A. PH Changes in the Micelle-Water Interface of Surface-Active Ionic Liquids Dictate the Stability of Encapsulated Curcumin: An Insight through a Unique Interfacial Reaction between Arenediazonium Ions and t-Butyl Hydroquinone. ACS Omega 2021, 6 (23), 14985–15000.
- (48) Finer, E. G.; Franks, F.; Tait, M. J. Nuclear Magnetic Resonance Studies of Aqueous Urea Solutions. *J. Am. Chem. Soc.* **1972**, *94* (13), 4424–4429.
- (49) Sinibaldi, R.; Ortore, M. G.; Spinozzi, F.; De Souza Funari, S.; Teixeira, J.; Mariani, P. SANS/SAXS Study of the BSA Solvation Properties in Aqueous Urea Solutions via a Global Fit Approach. *Eur. Biophys. J.* **2008**, *37* (5), 673–681.
- (50) Ash, D. E. Structure and Function of Arginases. *J. Nutr.* **2004**, 134 (10 SUPPL.), 2760S–2764S.

☐ Recommended by ACS

Structure and Interactions in Perfluorooctanoate Micellar Solutions Revealed by Small-Angle Neutron Scattering and Molecular Dynamics Simulations Stu...

Samhitha Kancharla, Paschalis Alexandridis, et al.

APRIL 22, 2021 LANGMUIR

READ 🗹

The Amphoteric Surfactant N,N-Dimethyldodecylamine N-Oxide Unfolds β-Lactoglobulin above the Critical Micelle Concentration

Kayla D. Thompson, Jason A. Berberich, et al.

MARCH 24, 2022

LANGMUIR

READ 🗹

Fast and Robust Quantification of Detergent Micellization Thermodynamics from Isothermal Titration Calorimetry

Shih-Chia Tso, Chad A. Brautigam, et al.

DECEMBER 12, 2019 ANALYTICAL CHEMISTRY

READ 🗹

Self-Assembly and Thermodynamic Parameters of Amitriptyline Hydrochloride in Polar Organic Solvent-Water Mixed Media

Jackson Gurung and Ajmal Koya Pulikkal SEPTEMBER 09, 2019

JOURNAL OF CHEMICAL & ENGINEERING DATA

READ 🗹

Get More Suggestions >